



# Photoluminescence and intrinsic ferromagnetism of Fe doped zinc oxide

Bidyarani Maibam<sup>1</sup> · Saptaka Baruah<sup>1</sup> · Sanjeev Kumar<sup>1</sup> Received: 6 April 2020 / Accepted: 16 September 2020 / Published online: 21 September 2020  
© Springer Nature Switzerland AG 2020

## Abstract

Zn<sub>1-x</sub>Fe<sub>x</sub>O nanoparticles with different doping concentration i.e. ( $x=0, 0.01, 0.02, 0.03, 0.04, 0.05$ ) were successfully synthesized via hydrothermal method. The crystal structure, morphology, optical and magnetic properties were studied by X-ray diffraction, field emission scanning electron microscope, UV–visible, photoluminescence spectra (PL) and vibrating sample magnetometer. The experimental results show that all the samples possess a single phase hexagonal wurtzite structure, no impurity phase was observed. The crystallite size decreases with the increase in Fe concentration. Optical absorption analysis by UV–visible exhibits a slight blueshift in the bandgap with increasing doping concentration. PL spectra shows that the emission peak in the UV region is absent for all the samples. All the emission peaks are in the visible region. Shifting of PL emission peaks is not observed indicating that the intrinsic defects are consistent. The magnetic observation indicated that all the samples including pure zinc oxide exhibit room temperature ferromagnetism (RTFM). The observed RTFM is attributed to the bound magnetic polaron that arises due to the presence of singly ionized oxygen vacancy ( $V_o$ ) as indicated by PL spectra.

**Keywords** ZnO · Hydrothermal · Fe-doped · Photoluminescence · Magnetic properties

## 1 Introduction

Diluted magnetic semiconductors (DMSs) are the materials formed by replacing cations of nonmagnetic semiconductors by magnetic ions such as transition metals (TM) ions or rare earth ions [1]. Ferromagnetism observed in DMS has led to its intense research because of their potential applications in spintronic devices, which uses both the spin in magnetic materials and charge of electrons [2]. Moreover, doping of transition metal into wide band gap semiconductor also leads to the tuning of optical and ferromagnetic properties [3]. Intrinsic ferromagnetism with high Curie temperature (above room temperature) is the principal requirement of DMSs for the application in spintronic devices [4]. Thus, efforts are made to produce TM metal doped wide bandgap semiconductor exhibiting

room temperature ferromagnetism (RTFM). Zinc oxide (ZnO) is II–VI wide band gap ( $E_g \sim 3.37$  eV) and large exciton binding energy (60 meV) compound semiconductor with hexagonal wurtzite structure of  $P6_3mc$  space group [5]. Requirement of Curie temperature above room temperature (RT) and intrinsic ferromagnetism (FM), rather than the ferromagnetism because of magnetic clusters or secondary phases of dopants for spintronics application makes transition metal doped ZnO a favorable system owing to observation of RTFM in several ZnO based system including Mn-, Fe- and Co-doped ZnO [6]. Results quite contradictory to each other are reported for ferromagnetism in transition metal doped ZnO. Liu et al. [7] reported RTFM and explains it as the intrinsic property of Fe doped ZnO. Reports suggesting that transition metal does not play any role in the magnetism of Mn and Fe

✉ Sanjeev Kumar, sanjeev.kumar@rgu.ac.in | <sup>1</sup>Department of Physics, Center of Advance Research, Rajiv Gandhi University, Rono Hills, Itanagar, Arunachal Pradesh, India.



doped ZnO thin films are also available [8]. Bhargava et al. [9] observed ferromagnetism in Cr doped ZnO. Taher et al. [10] observed ferromagnetism in nanostructure Co-doped ZnO thin films reasonably caused by the oxygen vacancies introduced in the films during the hydrothermal growth. RTFM was also reported by Mishra et al. in Fe doped ZnO nanostructures synthesized using chemical root and attributed its cause to Zinc vacancy ( $Zn_i$ ) while Wei et al. also observed ferromagnetism in Fe doped ZnO and attributed it to secondary phase for high doping concentration [11, 12]. Even though large numbers of reports are available in literature, there is a conflict for the origin of observed room temperature ferromagnetism in the transition metal doped ZnO DMS.

In the present work, our aim is to provide a better understanding of the origin of room temperature ferromagnetism. For this purpose, diluted magnetic semiconductor  $Zn_{1-x}Fe_xO$  with different doping concentration ( $x=0, 0.01, 0.02, 0.03, 0.04, 0.05$ ) is synthesized via hydrothermal method. The magnetic property is studied by using vibrating sample magnetometer (VSM). The structure and surface morphology is investigated by X-ray diffraction (XRD) and field emission scanning electron microscope (FESEM). The optical properties are studied with the help of UV–visible and photoluminescence (PL) spectra.

## 2 Experimental details

$Zn_{1-x}Fe_xO$  ( $x=0, 0.01, 0.02, 0.03, 0.04, 0.05$ ) nanoparticles are prepared by hydrothermal method. An aqueous solution of 1 M zinc nitrate hexahydrate 5 M sodium hydroxide and 1 M ferric nitrate nonahydrate solutions are prepared in double distilled water. Zinc nitrate hexahydrate and ferric nitrate nonahydrate solutions are mixed according to the required amounts and stirred at room temperature. Sodium hydroxide solution is added dropwise to it. After being stirred for 2 h, the mixture is transferred into a 200 ml Teflon lined stainless steel autoclave and is kept in an oven at 100 °C for 6 h. It is then allowed to cool down naturally at room temperature. The obtained product is washed with distilled water and dried at 100 °C for 24 h. The samples are then heated at 500 °C for 2 h. Figure 1 shows the flowchart depicting hydrothermal method used for the synthesis of  $Zn_{1-x}Fe_xO$  ( $x=0, 0.01, 0.02, 0.03, 0.04, 0.05$ ).

The structural and morphological characterizations of the samples are performed using X-ray diffractometer (Model: Smartlab XRD) and field emission scanning electron microscope (FESEM, Model: Carl Zeiss Ultra Plus). The optical properties are studied by using UV–visible spectrophotometer (Model: Cary 60 UV–Vis) and photoluminescence spectrophotometer (Model: Cary Eclipse

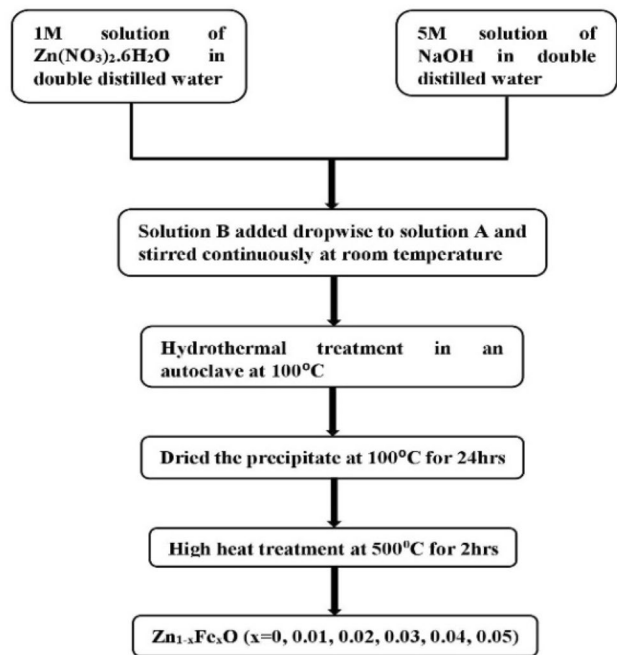


Fig. 1 Flowchart depicting hydrothermal method used for the synthesis of  $Zn_{1-x}Fe_xO$

Fluorescence Spectrophotometer). Vibrating sample magnetometer (VSM, Model: Quantum Design VERSALAB) was used for magnetic characterization.

## 3 Structural analysis

### 3.1 X-ray diffraction

Figure 2a shows the XRD pattern of  $Zn_{1-x}Fe_xO$  nanoparticles. The diffraction peaks in the XRD pattern corresponds to the diffraction of (100), (002), (101), (102), (110) planes indicating the formation of hexagonal wurtzite structure of ZnO with a space group  $P6_3mc$ . Furthermore, no traces of impurity or secondary phases within the detection limit of XRD and no obvious diffraction patterns of Iron (Fe) species such as Fe,  $Fe_2O_3$ , and  $Fe_3O_4$  are found in the samples of 1–5% Fe doped ZnO. The result indicates the successful incorporation of all Fe ions in the host ZnO crystal lattice. It is seen from the XRD pattern that with an increase Fe concentration the peak shifts towards the lower angle as compared to the pristine ZnO up to 3% doping and then again shift towards the higher angle being nearly equal to that for pristine ZnO at 4%. These results may be ascribed to the valence state of Fe ions. Fe ions are capable of existing as  $Fe^{2+}$ ,  $Fe^{3+}$  stably in compounds. In this paper, dopant ions are introduced into the host ZnO through ferric nitrate, so Fe would be in  $Fe^{3+}$  valence state. It is known that zinc act

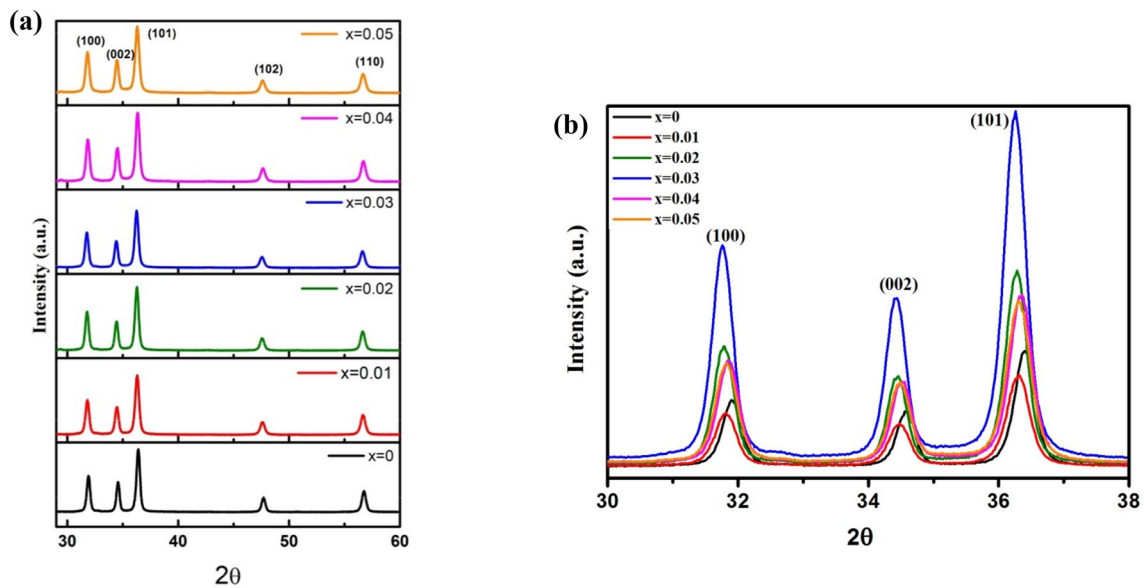


**Fig. 2** **a** XRD pattern of  $\text{Zn}_{1-x}\text{Fe}_x\text{O}$  ( $x=0, 0.01, 0.02, 0.03, 0.04, 0.05$ ). **b** XRD pattern of first three peaks of  $\text{Zn}_{1-x}\text{Fe}_x\text{O}$  ( $x=0, 0.01, 0.02, 0.03, 0.04, 0.05$ )

as a reducing agent in changing  $\text{Fe}^{3+}$ – $\text{Fe}^{2+}$  [24]. So, transition of  $\text{Fe}^{3+}$ – $\text{Fe}^{2+}$  is much expected as the host being ZnO in this case. The existence of Fe in  $\text{Fe}^{2+}$  is reported where the diffraction angle decreases with Fe concentration while the existence of iron as  $\text{Fe}^{3+}$  is reported where the diffraction angle increases [13–15]. Taking the peak position into consideration and from the existing reports, it can be inferred that  $\text{Fe}^{2+}$  and  $\text{Fe}^{3+}$  coexist in the Fe doped ZnO samples [16]. The shifting of peaks may also be due to the strain developed in the lattice due to doping. Broadening of peak, apart from its shift can be explained based on grain size reduction with Fe atom incorporation in ZnO. The ionic radii of  $\text{Fe}^{2+}$ ,  $\text{Fe}^{3+}$  and  $\text{Zn}^{2+}$  are 0.078, 0.068 and 0.074 nm respectively [17]. Substitution of  $\text{Zn}^{2+}$  with  $\text{Fe}^{2+}$ ,  $\text{Fe}^{3+}$  in the lattice site may cause lattice distortion resulting in strain in ZnO because of the difference in ionic radii of  $\text{Fe}^{2+}$  and  $\text{Fe}^{3+}$  with  $\text{Zn}^{2+}$  [18]. Fe ions need to have a balanced state of 2+ for maintaining the charge neutrality to properly substitute  $\text{Zn}^{2+}$  ionic sites. So, the balance state  $\text{Fe}^{3+}$  is likely to distort the lattice structure for maintaining the charge neutrality [19].

Figure 2b shows a large difference in intensity of XRD peaks for 1% and 3% Fe doped ZnO. The difference in intensity is due to the difference in their crystalline quality [13, 20]. The full width half maximum (FWHM) increases for 1% Fe doped ZnO indicating the decrease in the crystalline quality compares to pristine ZnO. The decrease in crystalline quality may be because of the lattice disorder and strain experience due to the incorporation of Fe ions in ZnO matrix [21]. But as the doping of Fe increases to 2%, FWHM value decreases suggesting

an increase in crystalline quality. The crystalline quality then again keeps on declining with the increase in doping up to 5% as implied by the increase in FWHM value. The increase in the crystallinity of the 2% Fe doped ZnO in our experiment may be ascribed to the formation of favorable nucleation centers from the dopant atoms for ZnO crystal growth. The decline in crystalline quality in 5% doping may be because of the saturation of newer nucleation centers or because of the ionic radii difference of  $\text{Zn}^{2+}$  and Fe ions [18]. Substitution of a large number of Fe ions in  $\text{Zn}^{2+}$  lattice sites leads to an increase in lattice distortion causing a larger strain which affects the crystal growth of ZnO.

The (101) preferred orientation with maximum intensity has been observed in the XRD pattern. The average crystallite size ( $D$ ) of the samples is estimated from XRD line width of (101) peak by using Scherrer's equation [22]. The crystalline size value of pristine and Fe doped ZnO is shown in Fig. 3. The crystallite size is in accordance with the FWHM values. The calculated values of  $a$ ,  $c$ ,  $c/a$ ,  $D$ ,  $d$ , volume, bond length, internal parameter ( $u$ ) and distortion degree ( $R$ ) are given in Table 1 [22].

The  $c/a$  ratio of pristine ZnO as well as Fe doped samples is less than the  $c/a$  ratio of ideal stoichiometry wurtzite structure ratio i.e. 1.633 indicating the presence of oxygen vacancies and zinc vacancies [23]. The calculated values of bond length vary from 1.9692 to 1.9735. Variation of bond length is not monotonous with doping concentration. The non-monotonous variation of bond length may be because of the strain present in the samples and a slight change in  $R$  is also observed [24].

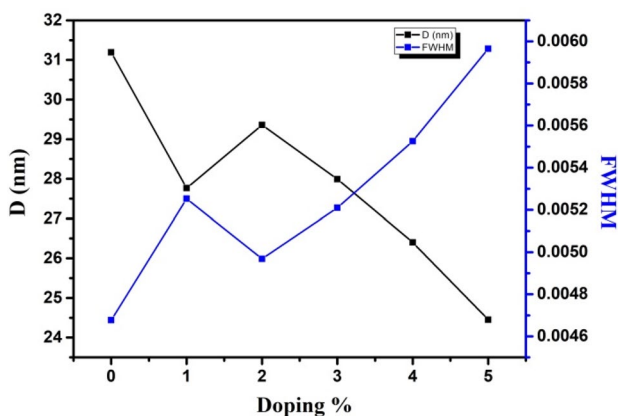


Fig. 3 Average crystallite size and FWHM of Zn<sub>1-x</sub>Fe<sub>x</sub>O (x=0, 0.01, 0.02, 0.03, 0.04, 0.05)

### 3.2 SEM analysis

The morphology of the synthesized Zn<sub>1-x</sub>Fe<sub>x</sub>O (x=0, 0.03, 0.05) materials are studied by field emission scanning electron microscope (FESEM). The FESEM images imply the change of shape and morphology of ZnO nanoparticles with doping. Figure 4a shows formation of a mixture of rod like and nanoflakes like morphology in pristine ZnO. In contrast, the Zn<sub>0.97</sub>Fe<sub>0.03</sub>O and Zn<sub>0.95</sub>Fe<sub>0.05</sub>O doped ZnO in Fig. 4b, c respectively showed cone-like particles that are formed may be due to the asymmetrical

and multidimensional growth of ZnO particles [25]. It is difficult to say something about the average grain size of the pristine and doped samples as the particles seems to be agglomerated for these images.

Energy dispersive X-ray analysis (EDAX) study is carried out for observing the elemental composition of synthesized samples and to verify the successful incorporation of dopants and the formation of ZnO nanoparticles. EDAX signals of pristine ZnO and Zn<sub>0.95</sub>Fe<sub>0.05</sub>O are shown in Fig. 5. For pristine ZnO nanoparticles, sharp signals of Zn and oxygen were found confirming the formation of ZnO nanoparticles. For Fe doped sample, Fe signals in addition to Zn and oxygen were also found, confirming the successfully incorporated of Fe in the ZnO.

## 4 Optical properties

### 4.1 UV-visible analysis

We explore and analyze pristine and Fe doped ZnO nanoparticles energy bandgap using UV-visible spectroscopy. The optical bandgap of the pristine and Fe doped sample is calculated by using the Tauc relation. Figure 6a shows the Tauc plot and the variation of bandgap with doping concentration is shown in Fig. 6b. Values of the bandgap are also tabulated in Table 2.

Table 1 Structural parameters of Zn<sub>1-x</sub>Fe<sub>x</sub>O (x=0, 0.01, 0.02, 0.03, 0.04, 0.05)

Zn <sub>1-x</sub> Fe <sub>x</sub> O	a=b (Å)	c (Å)	c/a	D (nm) (101)	d (Å) (101)	Volume (Å) <sup>3</sup>	Bond length (Å)	u	R
x=0	3.2355	5.1845	1.6024	31.1940	2.4653	47.0007	1.9692	0.379826	1.019122
x=0.01	3.2434	5.1961	1.6020	27.7665	2.47186	47.3385	1.9739	0.379879	1.019327
x=0.02	3.2474	5.1990	1.6009	29.3585	2.47318	47.4810	1.9759	0.38005	1.02
x=0.03	3.2494	5.2020	1.6009	27.9918	2.4745	47.5655	1.97708	0.380064	1.020055
x=0.04	3.2415	5.1845	1.5994	26.4017	2.46792	47.1743	1.9717	0.380303	1.020993
x=0.05	3.2435	5.1932	1.6011	24.4524	2.47186	47.3119	1.9735	0.380025	1.019901

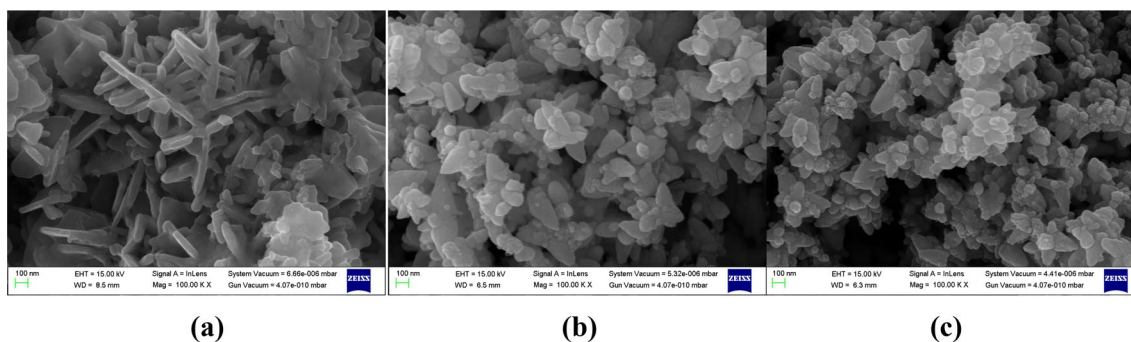


Fig. 4 SEM micrographs of Zn<sub>1-x</sub>Fe<sub>x</sub>O. a x=0, b x=0.03 and c x=0.05

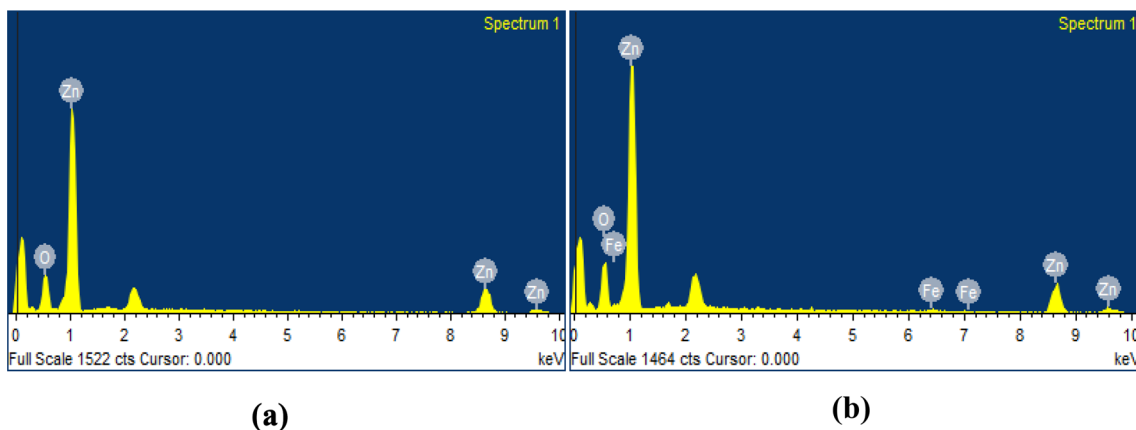


Fig. 5 EDAX pattern of Zn<sub>1-x</sub>Fe<sub>x</sub>O. **a** x=0 and **b** x=0.05

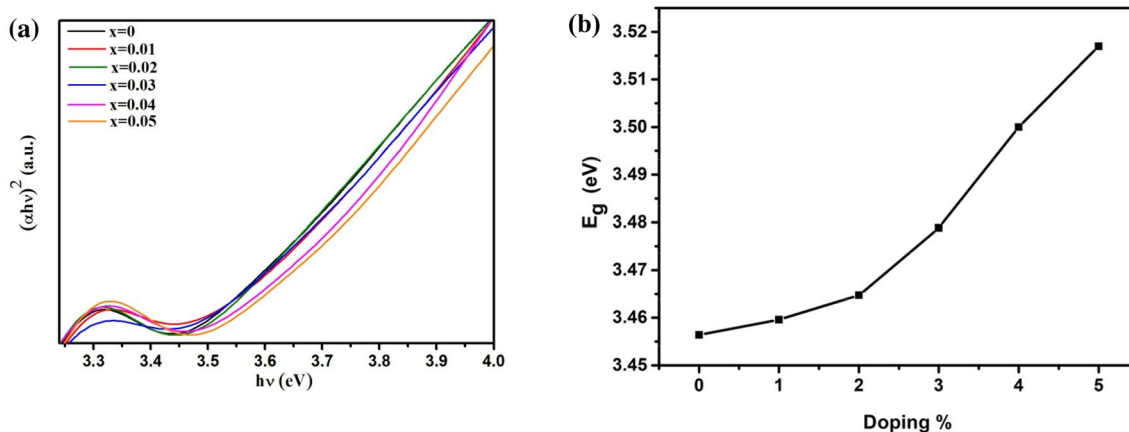


Fig. 6 **a** Band gap calculation of Zn<sub>1-x</sub>Fe<sub>x</sub>O (x=0, 0.01, 0.02, 0.03, 0.04, 0.05) nanoparticles and **b** doping percentage versus E<sub>g</sub>

**Table 2** Summary of bandgap (E<sub>g</sub>) of Zn<sub>1-x</sub>Fe<sub>x</sub>O (x=0, 0.01, 0.02, 0.03, 0.04, 0.05)

Zn <sub>1-x</sub> Fe <sub>x</sub> O	E <sub>g</sub> (eV)
x=0	3.456
x=0.01	3.459
x=0.02	3.464
x=0.03	3.478
x=0.04	3.5
x=0.05	3.516

The exciton Bohr radius of ZnO is much larger than the obtained average crystallite size. Therefore, the quantum confinement effect is not the major reason for the change in the bandgap of prepared samples [26]. The increase in bandgap may be due to the strain experienced by the doped sample. The result obtained is in agreement with the result reported by Parra-Palmino et al. [27] where they observed a large blueshift in

bandgap as the concentration of the dopant increase. The obtained bandgap is also in accordance with the result obtained by Hammad et al. [15] who explain the blue shift behavior based on Moss–Burstein theory. According to this theory, ZnO nanoparticle is *n*-type semiconductor and due to doping the Fermi level shifts inside the conduction band. The absorption edge shifts to higher energy as the states below such shifting in the conduction band are filled leading to the widening of bandgap. The shifting of Fermi level towards the conduction band may be attributed to the additional carriers or *d-d* transition from Fe. Rekha et al. and Arun et al. also explain the blue shift behavior of their sample based on the Moss–Burstein theory [28, 29]. The increase in bandgap or the blue shift behavior for the Fe doped sample with respect to that of pristine ZnO may also be because of the *sp-d* exchange interaction of localized *d* electron and band electrons as explained by Pal Singh et al. [30].



## 4.2 Photoluminescence (PL) characteristic

The PL properties of pristine and Fe-doped ZnO nanoparticles are also studied. The photoluminescence is recorded at room temperature with an excitation wavelength of 330 nm. Figure 7 shows the PL spectra at RT for all the samples. The inset of Fig. 7 represents the PL spectra of pristine ZnO deconvoluted into six peaks. Even though PL spectra of ZnO have been studied extensively, the source of visible range emission bands remains controversial. The typical photoluminescence spectra of ZnO have emission bands in the UV and visible regions. Usually, the UV luminescence peak is considered as the characteristics emission of ZnO and it is ascribed to the band edge emission or transition of exciton [31]. It is exciting to note that there is no UV emission peak in the PL spectra of prepared samples. This signifies that the recombination of exciton pairs of the prepared samples occurs at the non-radiative centers [32]. The disappearance of UV emission peak may also be attributed to a much higher intensity of visible emission due to an increase in defect density or it may also be because its excitation energy is significantly lower than its bandgap energy [33].

PL spectra confirmed that all the samples exhibited six peaks in the visible region. The peak near 416 nm (2.98 eV) in the PL spectra arises due to violet emission. This may arise because of the transition from conduction band (CB) to deep holes trapped levels above the valence band (VB) [34]. A single distinct peak centered about 458 nm (2.70 eV) in the blue band (2.75–2.63 eV) may be attributed to the direct recombination of a conduction electron in the CB and a hole in the VB [35]. The blue green emission peak centered about 486 nm (2.55 eV) may occur

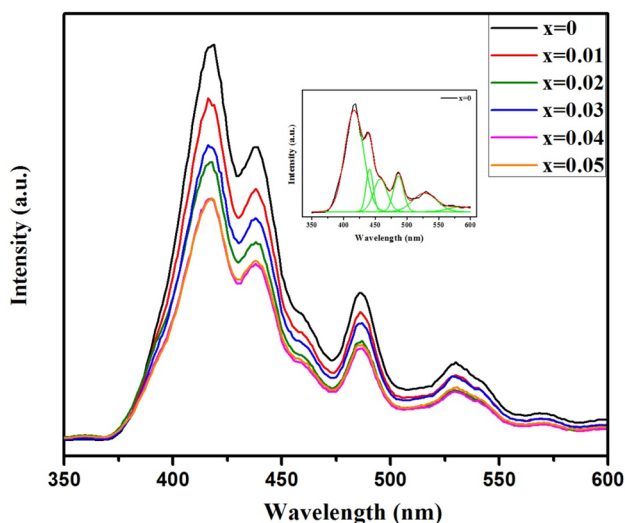


**Fig. 7** PL spectra of  $\text{Zn}_{1-x}\text{Fe}_x\text{O}$  ( $x=0, 0.01, 0.02, 0.03, 0.04, 0.05$ ) and the inset represents the deconvoluted spectra of pure ZnO

because of the electronic transition of donor level  $\text{Zn}_i$  to acceptor level Zinc vacancy ( $V_{\text{Zn}}$ ) [36]. Green emission peak centered about 528 nm (2.35 eV) is credited to defects related to oxygen vacancies because of the recombination of photogenerated holes and electron trapped by singly ionized oxygen vacancies ( $V_{\text{O}}$ ) [37].  $V_{\text{O}}$  are known as color centers (or F centers) and are also an important set of point defects in oxides. In the ZnO lattice, it shows three dissimilar charged states as  $F^{++}$ ,  $F^+$ ,  $F^0$ . The  $F^+$  oxygen vacancy which is singly occupied can contribute in activating bound magnetic polarons (BMP) and magnetic moment in DMSs. However,  $F^{++}$  and  $F^0$  vacancies do not induce FM in ZnO since they have spin zero ground states [14]. The broad peak centered about 584 nm (2.12 eV) in the range 550–600 nm (2.25–2.06 eV) is dedicated to the defect related transition originating from excess oxygen. Non-shifting of luminescence peaks in the visible range indicates that the intrinsic defects are consistent in all the samples [24]. Quenching of the luminescence peaks may be because of non-radiative recombination or may be due to the preferential occupation of  $\text{Fe}^{3+}$  ions by photogenerated electrons inducing trap centers [38].

## 5 Magnetic properties

To study the effect of Fe doping on the magnetic behavior of ZnO, the magnetization versus applied magnetic field curve obtain from VSM data performed at RT is studied. Figure 8 shows the M–H curves of  $\text{Zn}_{1-x}\text{Fe}_x\text{O}$  ( $x=0, 0.01, 0.02, 0.03, 0.04, 0.05$ ) nanoparticles. It is observed that the M–H curves of the pristine and doped samples do not saturate even at high applied fields. The M–H curve for all the samples comprises a linear part possibly because of the small paramagnetic (PM) and superparamagnetic (SPM) contribution in addition to a distinct ferromagnetic ordering confirmed by hysteresis behavior of the curve at lower field region [39]. Pristine ZnO ferromagnetism termed as  $d^0$  ferromagnetism may arise because of the presence of  $V_{\text{O}}$  defects and is supported by the PL spectra [40]. There are also reports indicating the role of  $\text{Zn}_i$  and  $V_{\text{O}}$  in maintaining pure ZnO magnetic behavior. RTFM may be due to extrinsic phenomena such as the formation of cluster or secondary phase of dopant ions and intrinsic phenomena such as exchange interaction [30]. The XRD pattern indicates that there is no formation of secondary phases such as  $\text{Fe}_2\text{O}_3$ ,  $\text{Fe}_3\text{O}_4$ , etc. Therefore, the observed ferromagnetism in our sample cannot be attributed to the formation of the secondary phase or cluster due to the doping of Fe. So, it may be because of the intrinsic phenomena and not due to the extrinsic phenomena. Number of models and concepts has been proposed to explain the room temperature ferromagnetism such as (a) hole mediated

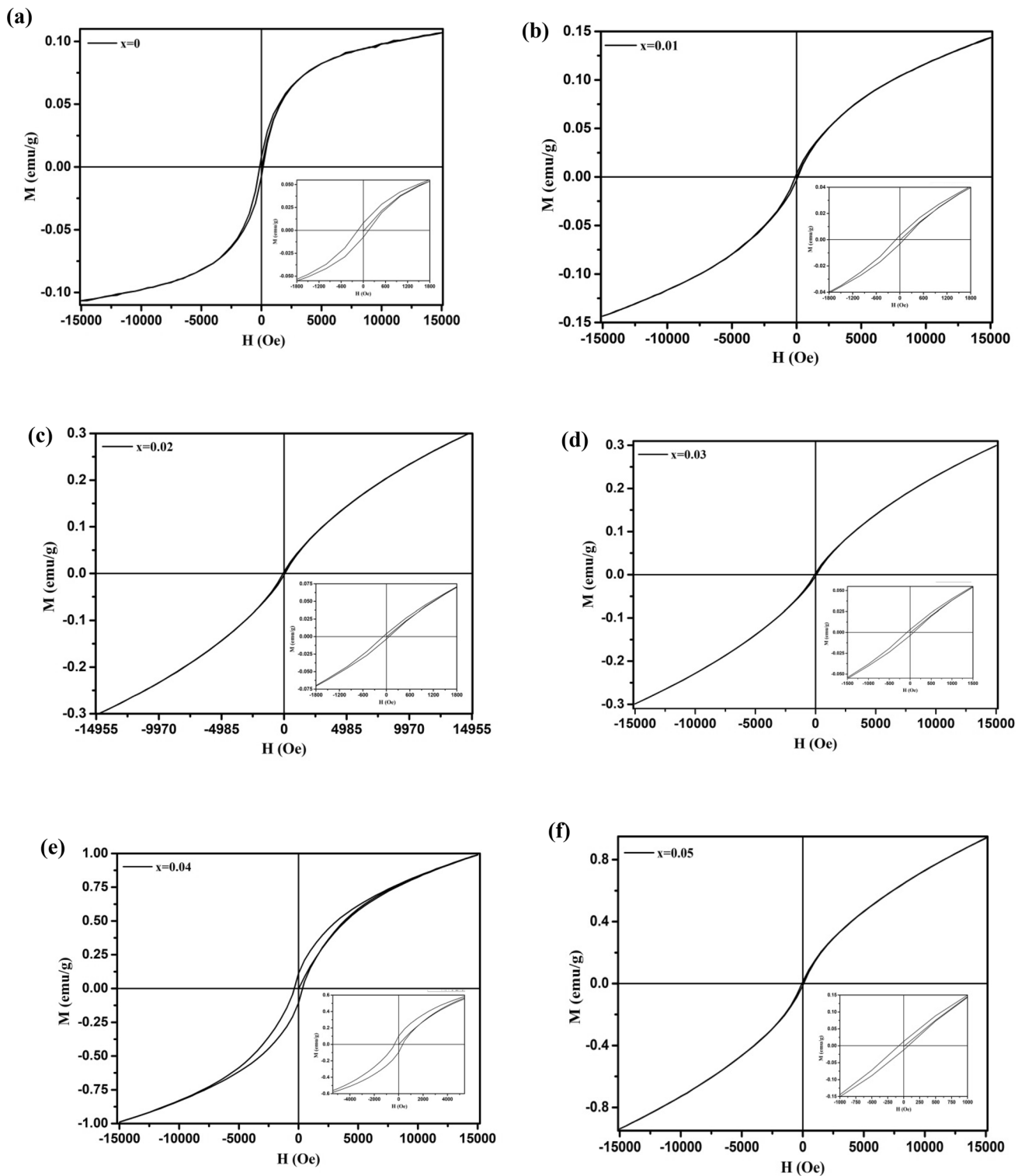


**Fig. 8** a–f  $M-H$  curve of  $Zn_{1-x}Fe_xO$  ( $x=0, 0.01, 0.02, 0.03, 0.04, 0.05$ ), the inset figure shows the enlarged  $M-H$  loop

Zener mean-field model (b) carrier-mediated RKKY (Ruderman–Kittel–Kasuya–Yosida) mechanism (c) donor impurity band exchange model, in this, the FM in DMSs is due to an indirect exchange donor electrons and this form a BMPs

and (d) direct interactions (such as double or superexchange mechanism). RKKY is not valid as it is based on free electrons and ZnO is a semiconductor and cannot be converted into metal, double exchange mechanism is also not

possible because of the very dilute doping of the sample [41]. Hole mediated Zener field model of ferromagnetism may also be excluded since ZnO is an *n*-type semiconductor [42]. So, the observed ferromagnetism for our sample can be centered on the substitutional behavior of Fe and can be understood based on bound magnetic polarons (BMPs) due to defects.  $F^+$  is known to be paramagnetic that can activate bound magnetic polaron and these BMPs interact leading to the formation of magnetic domains [43]. As a result, the singly occupied  $V_o$  may assume to be the cause of ferromagnetism. The interaction between  $V_o$  and Fe ions may lead to the formation of BMP in doped samples. The saturation magnetization ( $M_s$ ) is obtained by drawing a tangential line from the high field loop to the zero-field and is extrapolated. The intercept of the tangent on magnetization axis is taken as the value of  $M_s$ .  $M_s$  value increases up to 4% Fe doped samples and then decreases for 5% Fe doped ZnO. The enhancement in magnetization may be because of the overlapping of more Fe ions into the ferromagnetic domain with the increase in volume occupied by BMPs in accordance with the explanation given by Hsu et al. for Co-doped ZnO [44]. The decrease in magnetization may be because of the random distribution of some Fe ions leading to the decrease in net magnetization as mention by Iqbal et al. [45]. The result obtained is in accordance with the report given by Agarwal [46] where they observed a decrease in magnetization at higher Cu concentration. Table 3 shows the value of saturation magnetization ( $M_s$ ), coercivity ( $H_c$ ), remanence ( $M_r$ ).

Models describing the FM and SPM/PM behavior of magnetization curves are not found. The non-saturating hysteresis loop is a phenomenon commonly observed in thin films magnetic oxides. The slope of non-saturation term is known as high field susceptibility. Non-saturation of magnetization is also observed by Margulies [47] in  $Fe_3O_4$  films grown by sputter deposition on crystalline substrate and is term as anomalous. The approach to saturation magnetization problem has been discussed in detail by Chakazumi and Charap [48].

Assuming that the presence of restoring force increases with the advance of magnetization towards saturation,

the law of approach to saturation magnetization can be expressed as

$$M = Q \left( 1 - \frac{a}{\sqrt{H}} - \frac{b}{H} - \frac{c}{H^2} - \dots \right) + eH$$

where  $M$  is the actual magnetization value observe at  $H$  and the value of constant  $Q$  corresponds to its saturation value.  $a$ ,  $b$ ,  $c$  and  $e$  are constants. The term  $\frac{a}{\sqrt{H}}$  is credited to the point defects or magnetic anisotropy fluctuation on the atomic scale. The term  $\frac{b}{H}$  originated from the local internal stresses caused by dislocation and to voids or non-magnetic inclusions.  $\frac{c}{H^2}$  is credited to the weak and large scale fluctuations in the bulk anisotropy. The last term  $eH$  is negligible and hence ignored. It is caused by spontaneous magnetization by the external field. The high field susceptibility fitting curve is shown in Fig. 9. Table 4 shows the value of  $Q$ ,  $a$ ,  $b$ , and  $c$ .

## 6 Conclusion

In this work structural, optical and magnetic properties of  $Zn_{1-x}Fe_xO$  ( $x=0, 0.01, 0.02, 0.03, 0.04, 0.05$ ) nanoparticles synthesized by hydrothermal method has been studied. XRD results show that the particles exhibited a hexagonal wurtzite structure without any impurity phase and suggest that  $Fe^{2+}$  and  $Fe^{3+}$  ion coexist. Blueshift of optical band gap has been observed for the increase in Fe concentration. PL spectra show the absence of near band edge and all the observed emission peaks are in the visible region. Weak room temperature ferromagnetism even for the pure ZnO has been observed. The observed hysteresis loop has not been saturated even at high field, may be due to PM and SPM contribution. The observed ferromagnetism is intrinsic and is attributed to BMP.

**Table 3** summary of  $M_s$ ,  $H_c$ ,  $M_r$ ,  $M_r/M_s$  of  $Zn_{1-x}Fe_xO$  ( $x=0, 0.01, 0.02, 0.03, 0.04, 0.05$ )

$Zn_{1-x}Fe_xO$	$M_s$ (emu/g)	$H_c$ (Oe)	$M_r$ (emu/g)	$M_r/M_s$
$x=0$	0.08056	147.63	0.0082	0.10179
$x=0.01$	0.08792	106.668	0.00326	0.03708
$x=0.02$	0.11985	80.702953	0.00385	0.03212
$x=0.03$	0.12492	81.247	0.00354	0.02834
$x=0.04$	0.5655	359.0395	0.113	0.19982
$x=0.05$	0.42228	79.6043	0.01267	0.03



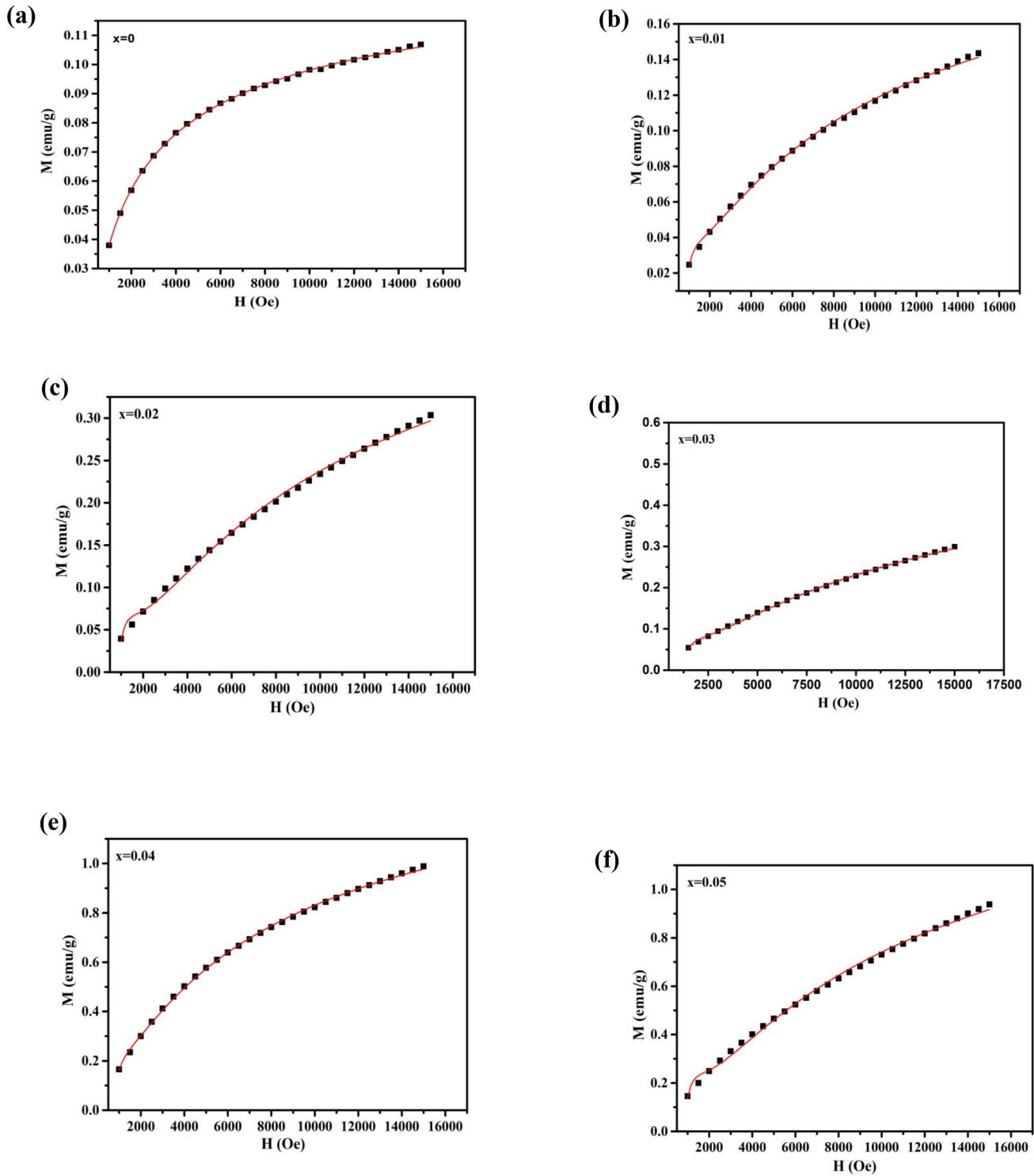


Fig. 9 a–f High field susceptibility fitting of  $Zn_{1-x}Fe_xO$  ( $x=0, 0.01, 0.02, 0.03, 0.04, 0.05$ )

**Table 4** Values of  $Q$ ,  $a$ ,  $b$ ,  $c$ 

Zn <sub>1-x</sub> Fe <sub>x</sub> O	$Q$	$a$	$b$	$c$
$x=0$	0.1484	39.6404	- 579.4606	70,772
$x=0.01$	0.2956	81.9868	- 2249.0897	575,636
$x=0.02$	0.7094	93.2831	- 2751.9501	750,506
$x=0.03$	0.7781	103.6176	- 3459.7957	1.2702E6
$x=0.04$	1.9021	74.4994	- 1858.4025	417,449
$x=0.05$	2.1417	91.8403	- 2718.9081	751,129

**Acknowledgements** Authors would like to acknowledge Dr. Naresh Kumar, MNNIT Allahabad, Prayagraj, India for providing the characterization facilities.

### Compliance with ethical standards

**Conflict of interest** The author(s) declare that they have no competing interests.

### References

- Chen AJ, Wu XM, Sha ZD, Zhuge LJ, Meng YD (2006) Structure and photoluminescence properties of Fe-doped ZnO thin films. *J Phys D Appl Phys* 39(22):4762
- Liu C, Yun F, Morkoc H (2005) Ferromagnetism of ZnO and GaN: a review. *J Mater Sci Mater Electron* 16(9):555
- Kumar S, Tiwari N, Jha SN, Chatterjee S, Bhattacharyya D, Sahoo NK, Ghosh AK (2015) Insight into the origin of ferromagnetism in Fe-doped ZnO diluted magnetic semiconductor nanocrystals: an EXFAS study of local structure. *RSC Adv* 5(115):94658–94669
- Sinha S, Singh M, Singh RP (2015) ZnO based diluted magnetic semiconductors for spintronic device applications: a review. *Int J Emerg Res Manag Technol* 4(7):16–20
- Benramache S, Arif A, Belahssen O, Guettaf A (2013) Study on the correlation between crystallite size and optical gap energy of doped ZnO thin film. *J Nanostruct Chem* 3(1):80
- Zhang ZH, Wang X, Xu JB, Muller S, Ronning C, Li Q (2009) Evidence of intrinsic ferromagnetism in individuals dilute magnetic semiconducting nanostructures. *Nat Nanotechnol* 4(8):523
- Liu H, Yang J, Zhang Y, Wang Y, Wei M (2008) Ferromagnetism and exchange bias in Fe-doped ZnO nanocrystals. *Mater Chem Phys* 112(3):1021–1023
- Hong NH, Sakai J, Brizé V (2007) Observation of ferromagnetism at room temperature in ZnO thin films. *J Phys Condens Matter* 19(3):036219
- Bhargava R, Sharma PK, Chawla AK, Kumar S, Chandra R, Pandey AC, Kumar N (2011) Variation in structural, optical and magnetic properties of Zn<sub>1-x</sub>Cr<sub>x</sub>O ( $x = 0.0, 0.10, 0.15, \text{ and } 0.20$ ) nanoparticles: role of dopant concentration on non-saturation of magnetization. *Mater Chem Phys* 125(3):664–671
- Taher FA, Abdeltwab E (2018) Shape-controlled synthesis of nanostructured Co-doped ZnO thin films and their magnetic properties. *CrystEngComm* 20(38):5844–5856
- Mishra AK, Das D (2010) Investigation on Fe-doped ZnO nanostructures prepared by a chemical route. *Mater Sci Eng B* 171(1–3):5–10
- Wei XX, Song C, Geng KW, Zeng F, He B, Pan F (2006) Local Fe structure and ferromagnetism in Fe-doped ZnO films. *J Phys Condens Matter* 18(31):7471
- Xu L, Li X (2010) Influence of Fe-doping on the structural and optical properties of ZnO thin films prepared by sol–gel method. *J Cryst Growth* 312(6):851–855
- Chen ZC, Zhuge LJ, Wu XM, Meng YD (2007) Initial study on the structure and optical properties of Zn<sub>1-x</sub>Fe<sub>x</sub>O films. *Thin Solid Films* 515(13):5462–5465
- Hammad TM, Griesing S, Wotocek M, Kuhn S, Hempelmann R, Hartmann U, Salem JK (2013) Optical and magnetic properties of Fe-doped ZnO nanoparticles prepared by the sol–gel method. *Int J Nanoparticles* 6(4):324
- Kim KJ, Park YR (2004) Optical investigation of Zn<sub>1-x</sub>Fe<sub>x</sub>O films grown on Al<sub>2</sub>O<sub>3</sub> (0001) by radio-frequency sputtering. *J Appl Phys* 96(8):4150–4153
- Abdel-Baset TA, Fang YW, Anis B, Duan CG, Abdel-Hafiez M (2016) Structural and magnetic properties of transition-metal-doped Zn<sub>1-x</sub>Fe<sub>x</sub>O. *Nanoscale Res Lett* 11(1):115
- Salaken SM, Farzana E, Podder J (2013) Effect of Fe-doping on the structural and optical properties of ZnO thin films prepared by spray pyrolysis. *J Semiconduct* 34(7):073003
- Cheng W, Ma X (2009) Structural, optical and magnetic properties of Fe-doped ZnO. *J Phys Conf Ser* 152(1):012039
- Kafle BP, Acharya S, Thapa S, Poudel S (2016) Structural and optical properties of Fe-doped ZnO transparent thin films. *Ceram Int* 42(1):1133–1139
- Wang C, Chen Z, He Y, Li L, Zhang D (2009) Structure, morphology and properties of Fe-doped ZnO films prepared by facing-target magnetron sputtering system. *Appl Surf Sci* 255(15):6881–6887
- Cullity BD (1956) Elements of X-ray diffraction. Addison-Wesley Publishing, Boston, MA
- Beltrán JJ, Barrero CA, Punnoose A (2015) Understanding the role of iron in the magnetism of Fe doped ZnO nanoparticles. *Phys Chem Chem Phys* 17(23):15284–15296
- Srivastava A, Kumar N, Khare S (2014) Enhancement in UV emission and bandgap by Fe doping in ZnO thin films. *Opto-Electron Rev* 22(1):68–76
- Pung SY, Lee WP, Aziz A (2012) Kinetic study of organic dye degradation using ZnO particles with different morphologies as a photocatalyst. *Int J Inorg Chem*. <https://doi.org/10.1155/2012/608183>
- Sharma D, Jha R (2017) Transition metal (Co,Mn) co-doped ZnO nanoparticles: effect on structural and optical properties. *J Alloys Compd* 698:532–538
- Parra-Palomino A, Perales-Perez O, Singhal R, Tomar M, Hwang J, Voyles PM (2008) Structural, optical, and magnetic characterization of monodisperse Fe-doped ZnO nanocrystals. *J Appl Phys* 103(7):07D121
- Rekha K, Nirmala M, Nair MG, Anukaliani A (2010) Structural, optical, photocatalytic and antibacterial activity of zinc oxide and manganese doped zinc oxide nanoparticles. *Phys B* 405(15):3180–3185
- Menon AS, Kalarikkal N, Thomas S (2013) Studies on structural and optical properties of ZnO and Mn-doped ZnO nanoparticles. *Indian J Nanosci* 1(1):16–24
- Singh RPP, Hudiara IS, Rana SB (2016) Effect of calcination temperature on the structural, optical and magnetic properties of pure and Fe-doped ZnO nanoparticles. *Mater Sci Poland* 34(2):451–459
- Lu YM, Li XP, Cao PJ, Su SC, Jia F, Han S, Liu WJ, Zhu DL, Ma XC (2012) Study of ultraviolet emission spectra in ZnO thin films. *J Spectrosc*. <https://doi.org/10.1155/2013/797232>

32. Ischenko V, Polarz S, Grote D, Stavarache V, Fink K, Driess M (2005) Zinc oxide nanoparticles with defects. *Adv Funct Mater* 15(12):1945–1954
33. Dorrastian D, Solati E, Dejam L (2012) Photoluminescence of ZnO nanoparticles generated by laser ablation in deionized water. *Appl Phys A* 109(2):307–314
34. Kundu S, Sain S, Satpati B, Bhattacharyya SR, Pradhan SK (2015) Structural interpretation, growth mechanism and optical properties of ZnO nanorods synthesized by a simple wet chemical route. *RSC Adv* 5(29):23101–23113
35. Wu X, Wei Z, Zhang L, Wang X, Yang H, Jiang J (2014) Optical and magnetic properties of Fe doped ZnO nanoparticles obtained by hydrothermal synthesis. *J Nanomater* 2014:1–6
36. Ghosh A, Choudhary RNP (2009) Structural evolution and visible photoluminescence of ZnO nanophosphor. *Phys Status Solidi (a)* 206(3):535–539
37. Das J, Mishra DK, Srinivasu VV, Sahu DR, Roul BK (2015) Photoluminescence and Raman studies for the confirmation of oxygen vacancies to induce ferromagnetism in Fe doped Mn:ZnO compound. *J Magn Magn Mater* 382:111–116
38. Ovhal MM, Kumar AS, Khullar P, Kumar M, Abhyankar AC (2017) Photoluminescence quenching and enhanced spin relaxation in Fe doped ZnO nanoparticles. *Mater Chem Phys* 195:58–66
39. Chanda A, Gupta S, Vasundhara M, Joshi SR, Mutta GR, Singh J (2017) Study of structural, optical and magnetic properties of cobalt doped ZnO nanorods. *RSC Adv* 7(80):50527–50536
40. Sundaresan A, Bhargavi R, Rangarajan N, Siddesh U, Rao CNR (2006) Ferromagnetism as a universal feature of nanoparticles of the otherwise nonmagnetic oxides. *Phys Rev B* 74(16):161306
41. Rana AK, Kumar Y, Rajput P, Jha SN, Bhattacharyya D, Shirage PM (2017) Search for the origin of room temperature ferromagnetism properties in Ni-doped ZnO nanostructure. *ACS Appl Mater Interfaces* 9(8):7691–7700
42. Ramay SM, Saleem M, Atiq S, Siddiqi SA, Imran M, Al-Zeghayer YS, Al-Awadi AS, Haider S, Mahmood A (2017) RKKY magnetic interactions in chemically synthesized  $Zn_{0.95-x}Fe_{0.05}Al_xO$  ( $x = 0, 0.03, 0.05, 0.07$ ) nanocrystallites. *Arab J Chem* 10:S1204–S1208
43. Zhan P, Wang W, Liu C, Hu Y, Li Z, Zhang Z, Zhang P, Wang B, Cao X (2012) Oxygen vacancy-induced ferromagnetism in un-doped ZnO thin films. *J Appl Phys* 111(3):033501
44. Hsu HS, Huang JCA, Huang YH, Liao YF, Lin MZ, Lee CH, Lee JF, Chen SF, Lai LY, Liu CP (2006) Evidence of oxygen vacancy enhanced room-temperature ferromagnetism in Co-doped ZnO. *Appl Phys Lett* 88(24):242507
45. Iqbal J, Wang B, Liu X, Yu D, He B, Yu R (2009) Oxygen-vacancy-induced green emission and room-temperature ferromagnetism in Ni-doped ZnO nanorods. *New J Phys* 11(6):063009
46. Agarwal DC, Singh UB, Gupta S, Singhal R, Kulriya PK, Singh F, Tripathi A, Singh J, Joshi US, Avasthi DK (2019) Enhanced room temperature ferromagnetism and green photoluminescence in Cu doped ZnO thin film synthesised by neutral beam sputtering. *Sci Rep* 9(1):1–12
47. Margulies DT, Parker FT, Spada FE, Goldman RS, Li J, Sinclair R, Berkowitz AE (1996) Anomalous moment and anisotropy behavior in  $Fe_3O_4$  films. *Phys Rev B* 53(14):9175
48. Chikazumi S (1955) *Physics of magnetism* (Wiley, New York, 1964), p. 554. W. Känzig, *Phys Rev* 9: 98–549

**Publisher's Note** Springer Nature remains neutral with regard to jurisdictional claims in published maps and institutional affiliations.